Laser-induced torques in spin spirals

Frank Freimuth [1,2,*] Stefan Blügel [1] and Yuriy Mokrousov [1,2]

[1] *Peter Grünberg Institut and Institute for Advanced Simulation, Forschungszentrum Jülich and JARA, 52425 Jülich, Germany*

[2] *Institute of Physics, Johannes Gutenberg University Mainz, 55099 Mainz, Germany*

(Received 27 November 2020; revised 15 January 2021; accepted 22 January 2021; published 2 February 2021)

We investigate laser-induced torques in magnetically noncollinear ferromagnets with a spin-spiral magnetic structure using *ab initio* calculations. Since spin spirals may be used to approximate the magnetization gradients locally in domain walls and skyrmions, our method may be used to obtain the laser-induced torques in such objects from a multiscale approach. Employing the generalized Bloch theorem, we obtain the electronic structure computationally efficiently. We employ our method to assess the laser-induced torques in bcc Fe, hcp Co, and $L_1 0$ FePt when a spin-spiral magnetic structure is imposed. We find that the laser-induced torques in these magnetically noncollinear systems may be orders of magnitude larger than those in the corresponding magnetically collinear systems and that they exist for both linearly and circularly polarized light. This result suggests that laser-induced torques driven by noncollinear magnetic order or by magnetic fluctuations may contribute significantly to processes in ultrafast magnetism.

DOI: 10.1103/PhysRevB.103.054403

I. INTRODUCTION

Femtosecond laser pulses exert effective magnetic fields on the magnetization in collinear ferromagnets, which may be used to tilt the magnetization and to excite magnetization dynamics [1–3]. These effective magnetic fields have been ascribed to the inverse Faraday effect (IFE) and to the optical spin transfer torque (OSTT) [4–7]. The IFE is a key ingredient in several theoretical explanations of magnetization reversal in ferromagnetic thin films [8,9].

In spintronics, the spin-orbit torque [10] requires spin-orbit interaction (SOI), while the spin-transfer torque [11] does not. The reason is that in collinear ferromagnets the angular momentum can be transferred only to the lattice, which requires SOI, while in noncollinear magnets, spin valves, and magnetic tunnel junctions the angular momentum is transferred between different magnetization directions and between different magnetic layers, which does not require SOI. IFE and OSTT have been studied mostly in collinear magnets, and they require SOI.

This comparison between spintronics and laser-induced ultrafast magnetism therefore poses the question of whether there are additional laser-induced torques in noncollinear magnets or in spin valves that arise from different mechanisms than the IFE and the OSTT. Indeed, laser pulses may distort domain walls and excite magnetization dynamics in them [12,13]. Additionally, laser pulses excite spin currents in spin valves, which generate spin-transfer torques when they flow between different magnetic layers [14,15]. These laser-induced spin-transfer torques resemble the Slonczewski spin-transfer torque in spintronics. However, in spintronics a second type of torque is known, the so-called nonadiabatic torque [11,16–19]. Therefore, one may expect that not only the Slonczewski torque but also the nonadiabatic torque should have a laser-induced counterpart in ultrafast magnetism. We will confirm this expectation in this paper.

Strong femtosecond laser pulses not only generate effective magnetic fields; they also trigger ultrafast demagnetization. There are many indications that ultrafast demagnetization in transition metal collinear ferromagnets is not dominated by collapsed exchange but rather by collective excitations [20–22]. Since the magnetization is noncollinear in the presence of collective excitations, one may pose the question of whether the laser-induced torques that arise from this noncollinearity might contribute to the ultrafast demagnetization itself. Moreover, in order to describe the processes involved in ultrafast magnetism at room temperature properly, it is crucial to take the initial thermal fluctuations of the magnetization into account [23,24]. Within the limitations of the frozen magnon approximation our results on spin spirals may also be used to estimate the laser-induced torques on magnons, which therefore provides a valuable asset to understand the torques active in ultrafast magnetism.

Several recent works have added an ultrafast-magnetism perspective to magnetically noncollinear objects such as skyrmions [25–27] and domain walls [12,13]. In order to apply our results for homogeneous spin spirals to such inhomogeneous objects one may locally approximate the magnetization gradients by spin spirals and use a multiscale approach [28].

This paper is structured as follows. In Sec. II we present our theory and computational formalism of laser-induced torques in spin spirals. In Sec. II A we introduce basic notations. In Sec. II B we discuss the symmetry properties of laser-induced torques. In Sec. II C we explain the key differences between laser-induced torques on spin spirals and the current-induced torques known from spintronics. In Sec. II D we develop a

*Corresponding author: f.freimuth@fz-juelich.de

simple model useful to understand laser-induced torques on spin spirals. In Sec. II E we describe how key properties of the laser-induced torques may be understood within the gauge-field approach. In Sec. II F we describe our computational method. In Sec. III we discuss our *ab initio* results for the laser-induced torques in bcc Fe, hcp Co, and $L1_0$ FePt. This paper ends with a summary in Sec. IV.

II. THEORY

A. Laser-induced torques on spin spirals

The magnetization direction $\hat{\boldsymbol{M}}$ of spin spirals may be written as

$$\hat{\boldsymbol{M}}(\boldsymbol{r}) = \mathcal{R}(\alpha, \beta)\begin{pmatrix}\sin(\theta)\cos(\boldsymbol{q}\cdot\boldsymbol{r}+\phi)\\ \sin(\theta)\sin(\boldsymbol{q}\cdot\boldsymbol{r}+\phi)\\ \cos(\theta)\end{pmatrix}, \tag{1}$$

where $\boldsymbol{q}$ is the spin-spiral wave vector, θ is the cone angle of the spin spiral, and $\mathcal{R}(\alpha, \beta)$ is a proper orthogonal rotation matrix parameterized by the two Euler angles, α and β. When $\alpha = \beta = 0$, we have $\mathcal{R}(0, 0) = 1$, and Eq. (1) describes a helical spin spiral when $\theta = 90^\circ$ and when $\boldsymbol{q}$ points in the z direction. When $\boldsymbol{q}$ lies in the xy plane, it describes a cycloidal spiral. Nonzero Euler angles are needed in Eq. (1) to describe, e.g., a helical spin spiral propagating in the x direction or a cycloidal spin spiral propagating in the z direction.

Since torques on the magnetization are perpendicular to it, any torque on the magnetization of a spin spiral may be expressed as

$$\boldsymbol{T}(\boldsymbol{r}) = \mathcal{R}(\alpha, \beta)[\hat{\boldsymbol{e}}_\theta(\boldsymbol{r})T_\theta + \hat{\boldsymbol{e}}_\phi(\boldsymbol{r})T_\phi], \tag{2}$$

where the unit vectors $\hat{\boldsymbol{e}}_\theta(\boldsymbol{r})$ and $\hat{\boldsymbol{e}}_\phi(\boldsymbol{r})$ are given by

$$\hat{\boldsymbol{e}}_\theta(\boldsymbol{r}) = \begin{pmatrix}\cos(\theta)\cos(\boldsymbol{q}\cdot\boldsymbol{r}+\phi)\\ \cos(\theta)\sin(\boldsymbol{q}\cdot\boldsymbol{r}+\phi)\\ -\sin(\theta)\end{pmatrix} \tag{3}$$

and

$$\hat{\boldsymbol{e}}_\phi(\boldsymbol{r}) = \begin{pmatrix}-\sin(\boldsymbol{q}\cdot\boldsymbol{r}+\phi)\\ \cos(\boldsymbol{q}\cdot\boldsymbol{r}+\phi)\\ 0\end{pmatrix}, \tag{4}$$

respectively.

In spintronics, current-induced contributions to the torque T_ϕ are referred to as the *adiabatic* torque, while current-induced contributions to T_θ are referred to as the *nonadiabatic* torque [11]. It is nowadays agreed that the terms *adiabatic* and *nonadiabatic* are not optimal to describe the mechanisms involved in these current-induced torques. However, these two terms are well established to distinguish the two possible directions of the current-induced torque. When a torque is generated by the application of laser light, this torque may be decomposed as well into the two components T_ϕ and T_θ, which we denote therefore *laser-induced adiabatic torque* and *laser-induced nonadiabatic torque*, respectively. However, while borrowing these terms from spintronics, we do not suggest that the microscopic origin of laser-induced torques is in any way similar to the microscopic origin of current-induced torques. The analogies between the two, which suggest using the terms *adiabatic* and *nonadiabatic* for both effects, are only in the geometry, i.e., in the directions of these two components, and in the effect of the torques on the magnetization dynamics. The difference in mechanisms is explored in Secs. II C and II D.

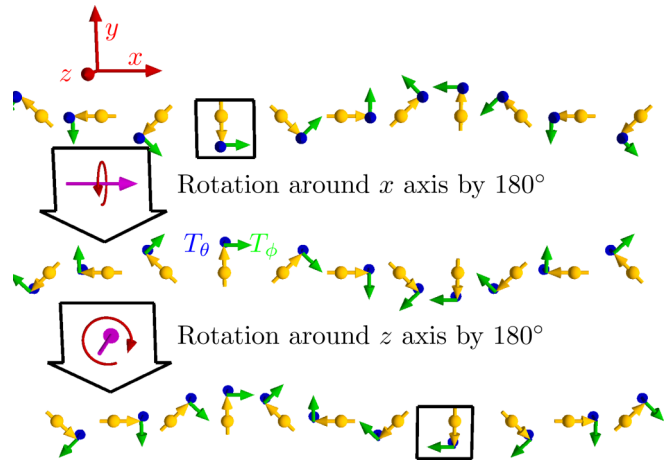

FIG. 1. Two consecutive 180° rotations around the x and z axes affect a flat spin spiral (yellow arrows) in the same way as a net translation of the spin spiral along the x direction does. However, these two consecutive rotations flip the signs of T_θ and T_ϕ (compare the torques, e.g., in the two square boxes). Consequently, symmetry requires the laser-induced torques to vanish in flat spin spirals.

B. Symmetry of laser-induced torques

Consider a flat spin spiral in the xy plane, i.e., $\theta = 90^\circ$, $\mathcal{R} = 1$, and $\boldsymbol{q}$ along the x direction in Eq. (1). Two subsequent rotations of the spin spiral, first by 180° around the x axis and then by 180° around the z axis, lead to a simple translation of the entire spin spiral (see Fig. 1). However, the application of these rotations to the torque reverses the sign of the torque. Therefore, the laser-induced torques vanish in this case. Generally, for flat spin spirals, i.e., when $\theta = 90^\circ$, the laser-induced torques vanish. Note that in this symmetry argument we do not consider SOI because in this work we consider only laser-induced torques that arise from the noncollinear magnetic order. In the presence of SOI the above symmetry argument does not hold because the two rotations are not allowed by symmetry.

Consider a Néel-like spiral with the q vector in the x direction, cone angle θ, and $\mathcal{R} = 1$ in Eq. (1) (see Fig. 2). When we rotate the spiral around the z axis by 180°, the q vector changes sign, but the torque is not modified. Consequently, laser-induced torques are even in q. However, when we rotate next around the x axis by 180°, the torque changes sign. Therefore, $\boldsymbol{T}(\theta) = -\boldsymbol{T}(180^\circ - \theta)$. This suggests that the dependence of the torques on θ may be described by $\propto \sin(2\theta)$ at the leading order. As a special case it follows that the torque vanishes when $\theta = 90^\circ$, consistent with the result above.

C. Current-induced vs laser-induced torques on spin spirals: Different mechanisms

While we borrowed the terms *adiabatic* and *nonadiabatic* from spintronics in order to distinguish the two components of the laser-induced torques, the mechanisms responsible for

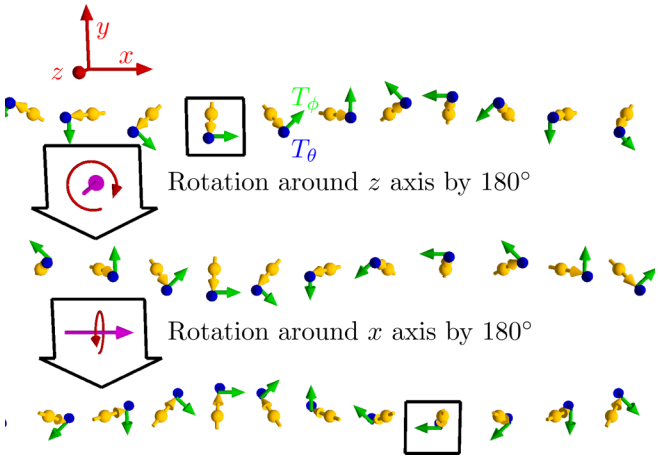

FIG. 2. A first rotation around the z axis by 180° flips the sign of the q vector of the spin spiral but does not affect the torques. Consequently, laser-induced torques are even in q. A second rotation around the x axis by 180° flips the sign of the torques (compare, e.g., the torques in the two square boxes). Consequently, the torques satisfy $\boldsymbol{T}(\theta) = -\boldsymbol{T}(180^\circ - \theta)$.

current-induced torques on spin spirals are quite different from those generating the laser-induced torques. In this section we explore some of these differences.

When an electric current propagates along a spin spiral, the spin current is given by

$$\boldsymbol{Q}_i(\boldsymbol{r}) = \frac{\hbar}{2e} P J_i \hat{\boldsymbol{M}}(\boldsymbol{r}). \tag{5}$$

Here, the vector $\boldsymbol{Q}_i(\boldsymbol{r})$ describes the spin current density flowing along the ith Cartesian direction. This vector is parallel to the orientation of the spin polarization of this spin current. J_i is the electric current density along the ith Cartesian direction, and

$$P = \frac{\sigma_\uparrow - \sigma_\downarrow}{\sigma_\uparrow + \sigma_\downarrow} \tag{6}$$

is its polarization. $\sigma_\uparrow$ and $\sigma_\downarrow$ are the respective contributions of the minority and majority electrons to the electrical conductivity. The resulting torque is given by

$$\boldsymbol{T}^{\text{adia}}(\boldsymbol{r}) = \sum_i \frac{\partial \boldsymbol{Q}_i}{\partial r_i}. \tag{7}$$

In Eq. (5) we assumed that the electron spin follows the local magnetization direction adiabatically. Therefore, the torque in Eq. (7) is called the adiabatic torque.

When a laser pulse is applied to a homogeneous spin spiral in a centrosymmetric crystal, inversion symmetry does not allow any spin current to be generated by the laser pulse at the second order of the electric field of the laser light. Of course, if the laser spot has a finite size, spin current will flow out of the illuminated region, but we consider here the situation where the entire spiral is homogeneously illuminated by the pulse. The absence of spin currents in homogeneously illuminated spin spirals shows that the microscopic mechanisms of laser-induced torques have to be different from those of current-induced torques in spin spirals. Certainly, there are several experiments where laser pulses excite superdiffusive spin currents, which exert torques on magnets [14]. However, in these experiments two magnets are separated by a nonmagnetic spacer, which is a geometry different from the one of a homogeneous spin spiral that we consider in this work.

Since the spin current cannot explain the laser-induced torque in homogeneous spin spirals, we develop a simple model in the following section.

D. Gradient expansion

The Kohn-Sham Hamiltonian of a magnetic system may be written as

$$H(\boldsymbol{r}) = H_0(\boldsymbol{r}) - \boldsymbol{m} \cdot \hat{\boldsymbol{M}}(\boldsymbol{r}) \Omega^{\text{xc}}(\boldsymbol{r}), \tag{8}$$

where the first term, $H_0(\boldsymbol{r})$, contains kinetic energy and scalar potential, while the exchange interaction is described by the second term. Here, $\Omega^{\text{xc}}(\boldsymbol{r})$ is the exchange field, i.e., the difference between the potentials of majority and minority electrons $\Omega^{\text{xc}}(\boldsymbol{r}) = \frac{1}{2\mu_{\text{B}}}[V^{\text{eff}}_{\text{minority}}(\boldsymbol{r}) - V^{\text{eff}}_{\text{majority}}(\boldsymbol{r})]$; $\boldsymbol{m} = -\mu_{\text{B}}\sigma$; μ_{B} is the Bohr magneton; and $\sigma = (\sigma_x, \sigma_y, \sigma_z)^{\text{T}}$ is the vector of Pauli spin matrices.

In general the magnetization of a spin spiral, Eq. (1), breaks the translational invariance of the crystal lattice. In order to obtain at a position $\boldsymbol{r}_0$ a local Hamiltonian that is consistent with the crystal lattice translational symmetries one may expand the exchange interaction in $H(\boldsymbol{r})$ around $\boldsymbol{r}_0$. The expansion of the Hamiltonian around the position $\boldsymbol{r}_0$ is given by

$$\begin{aligned} H(\boldsymbol{r}) = {} & H_0(\boldsymbol{r}) - \boldsymbol{m} \cdot \hat{\boldsymbol{M}}(\boldsymbol{r}_0) \Omega^{\text{xc}}(\boldsymbol{r}) \\ & - \Omega^{\text{xc}}(\boldsymbol{r}) \frac{\partial \{\boldsymbol{m} \cdot \hat{\boldsymbol{M}}(\boldsymbol{r}_0)\}}{\partial \boldsymbol{r}_0} \cdot [\boldsymbol{r} - \boldsymbol{r}_0] \\ & - \frac{1}{2} \Omega^{\text{xc}}(\boldsymbol{r}) \sum_{ij} \frac{\partial^2 \{\boldsymbol{m} \cdot \hat{\boldsymbol{M}}(\boldsymbol{r}_0)\}}{\partial r_{0,i} \partial r_{0,j}} \\ & \times [r_i - r_{0,i}][r_j - r_{0,j}] + \cdots . \end{aligned} \tag{9}$$

Consequently, the local Hamiltonian at $\boldsymbol{r}_0$ is

$$\begin{aligned} \langle H(\boldsymbol{r}) \rangle \simeq {} & H_0(\boldsymbol{r}) - \boldsymbol{m} \cdot \hat{\boldsymbol{M}}(\boldsymbol{r}_0) \Omega^{\text{xc}}(\boldsymbol{r}) \\ & - \frac{1}{2} \Omega^{\text{xc}}(\boldsymbol{r}) \sum_{ij} \frac{\partial^2 \{\boldsymbol{m} \cdot \hat{\boldsymbol{M}}(\boldsymbol{r}_0)\}}{\partial r_{0,i} \partial r_{0,j}} \langle [r_i - r_{0,i}][r_j - r_{0,j}] \rangle \end{aligned} \tag{10}$$

because $\langle [\boldsymbol{r} - \boldsymbol{r}_0] \rangle = 0$ in systems with inversion symmetry. Here, $\langle \cdots \rangle$ denotes a suitable averaging.

The second derivative of the magnetization direction is given by

$$\begin{aligned} \frac{\partial^2 \hat{\boldsymbol{M}}(\boldsymbol{r}_0)}{\partial r_{0,i} \partial r_{0,j}} = {} & -q_i q_j \sin\theta [\sin\theta \hat{\boldsymbol{M}}(\boldsymbol{r}_0) \\ & + \cos\theta \mathcal{R}(\alpha, \beta) \hat{\boldsymbol{e}}_\theta(\boldsymbol{r}_0)], \end{aligned} \tag{11}$$

which leads to an effective magnetic field perpendicular to the local magnetization:

$$\boldsymbol{B}_{\boldsymbol{q}}(\boldsymbol{r}) = -b_{\boldsymbol{q}} \Omega^{\text{xc}}(\boldsymbol{r}) \sin(2\theta) \mathcal{R}(\alpha, \beta) \hat{\boldsymbol{e}}_\theta(\boldsymbol{r}), \tag{12}$$

where

$$b_{\boldsymbol{q}} = \frac{1}{4}\sum_{ij} q_i q_j \langle [r_i - r_{0,i}][r_j - r_{0,j}]\rangle. \tag{13}$$

Consequently, the local Hamiltonian may be written as

$$\langle H(\boldsymbol{r})\rangle \simeq H_0(\boldsymbol{r}) - \boldsymbol{m}\cdot[\hat{\boldsymbol{M}}(\boldsymbol{r}_0)\Omega^{\mathrm{xc}}(\boldsymbol{r}) + \boldsymbol{B}_{\boldsymbol{q}}(\boldsymbol{r})]. \tag{14}$$

We assume that the application of a laser pulse generates two torques, one in the direction of $\hat{\boldsymbol{M}}\times\boldsymbol{B}_{\boldsymbol{q}} \propto \hat{\boldsymbol{e}}_\phi$ and a second one in the direction of $\hat{\boldsymbol{M}}\times[\hat{\boldsymbol{M}}\times\boldsymbol{B}_{\boldsymbol{q}}] \propto \hat{\boldsymbol{e}}_\theta$. According to Eq. (12), these torques are proportional to $\sin(2\theta)$, which is consistent with the symmetry analysis in Sec. II B. According to Eq. (13), these torques are even in $\boldsymbol{q}$, which is consistent with the symmetry analysis in Sec. II B and also with our *ab initio* results in Sec. III. Thus, the assumption that the interaction of laser-excited electrons with the effective magnetic field $\boldsymbol{B}_{\boldsymbol{q}}(\boldsymbol{r})$ leads to the laser-induced torques predicts a dependence on $\boldsymbol{q}$ and θ that agrees with the *ab initio* results. Clearly, $\boldsymbol{B}_{\boldsymbol{q}}(\boldsymbol{r})$ exists even without any applied laser pulse. However, the expectation value $\langle[r_i - r_{0,i}][r_j - r_{0,j}]\rangle$ in Eq. (13) is state dependent, and therefore, $b_{\boldsymbol{q}}$ changes when a laser pulse is applied.

When the q vector is equal to a primitive vector $\boldsymbol{b}$ of the reciprocal lattice, one picks up the phase 2π over the length of a primitive lattice vector. Consequently, $\boldsymbol{q} = \boldsymbol{b}$ describes the same magnetic structure as $\boldsymbol{q} = 0$. Similarly, $\boldsymbol{q} = \boldsymbol{b}/2$ describes an antiferromagnet, where neighboring magnetic atoms exhibit antiparallel magnetic moments. In such a collinear antiferromagnetic configuration the laser-induced torques are zero. Therefore, we expect the torques to increase first with increasing q, to attain a maximum around $\boldsymbol{b}/4$, and to decrease afterwards until they are zero at $\boldsymbol{b}/2$. Thus, the model developed in this section, which predicts that the torques increase with increasing q, is expected to be valid only for $q < \pi/(2a)$, where a is the lattice constant.

E. Gauge-field approach to spin spirals

The effects of magnetic texture on conduction electrons often resemble those of SOI. In fact, mathematical exact transformations of magnetization gradients into an effective SOI have been derived and exploited in important model systems (see Ref. [29] for a recent review). These relations have been used not only for the discussion of effects linear in the magnetization gradients but also for effects, e.g., quadratic in the magnetization gradients [30]. One may argue that this equivalence between magnetic noncollinearity and effective SOI explains why laser-induced torques exist in spin spirals even without real SOI, while collinear ferromagnets exhibit nonzero laser-induced torques only in the presence of SOI: Instead of the real SOI it is the effective SOI due to the magnetic noncollinearity that generates these torques in spin spirals even without any real atomic SOI. This argument has been used to predict an IFE in topological magnetic structures even without SOI [31].

In this work we consider Fe, Co, and FePt. In these materials the SOI strength on the magnetic atom is of the order of 60 meV. Using the gauge-field approach from Ref. [32], we estimate that noncollinearity produces an effective SOI of the order of magnitude of

$$\frac{\hbar^2 q k}{2m} \approx 1.5\,\mathrm{eV}, \tag{15}$$

where we set $q = k = 2\pi/(10\ \text{Å})$. This is larger than the real SOI by a factor of 25. Consequently, we expect the laser-induced torques from noncollinearity to be larger than those from real SOI in these materials.

In Secs. II B and II D we showed that the laser-induced torques in spin spirals are expected to be even in the q vector and to exhibit the angular dependence $\propto \sin(2\theta)$. In the following we show how these dependences may be understood within the gauge-field approach. Using a gauge transformation, the Hamiltonian in Eq. (8) may be rewritten as follows [we set $\mathcal{R} = 1$ and $\phi = 0$ in Eq. (1)] [19,32,33]:

$$H(\boldsymbol{r}) = H_0(\boldsymbol{r}) - \boldsymbol{m}\cdot\hat{\boldsymbol{M}}^{\mathrm{eff}}\Omega^{\mathrm{xc}}(\boldsymbol{r}) + e\boldsymbol{A}^{\mathrm{eff}}\cdot\boldsymbol{v}, \tag{16}$$

where $\boldsymbol{v}$ is the velocity operator,

$$\boldsymbol{A}^{\mathrm{eff}} = -\frac{i\hbar}{e}U^\dagger(\boldsymbol{r})\frac{\partial U(\boldsymbol{r})}{\partial \boldsymbol{r}} \tag{17}$$

is an effective vector potential, and

$$U(\boldsymbol{r}) = \begin{pmatrix} i\cos\frac{\boldsymbol{q}\cdot\boldsymbol{r}}{2} + \sin\frac{\boldsymbol{q}\cdot\boldsymbol{r}}{2} & 0 \\ 0 & \sin\frac{\boldsymbol{q}\cdot\boldsymbol{r}}{2} - i\cos\frac{\boldsymbol{q}\cdot\boldsymbol{r}}{2}\end{pmatrix} \tag{18}$$

transforms the noncollinear magnetization of the spin spiral into the collinear magnetization

$$\hat{\boldsymbol{M}}^{\mathrm{eff}} = (-\sin\theta, 0, \cos\theta)^{\mathrm{T}}. \tag{19}$$

Explicitly, the effective vector potential is given by

$$\boldsymbol{A}^{\mathrm{eff}} = \frac{\hbar}{e}\begin{pmatrix} -\frac{\boldsymbol{q}}{2} & 0 \\ 0 & \frac{\boldsymbol{q}}{2}\end{pmatrix}. \tag{20}$$

We denote the two eigenstates of the matrix

$$-\boldsymbol{m}\cdot\hat{\boldsymbol{M}}^{\mathrm{eff}} = \mu_{\mathrm{B}}\begin{pmatrix} \cos\theta & -\sin\theta \\ -\sin\theta & -\cos\theta\end{pmatrix} \tag{21}$$

by $|\uparrow\rangle$ and $|\downarrow\rangle$. Since $\hat{\boldsymbol{M}}^{\mathrm{eff}}$ lies in the xz plane, we have $\langle\uparrow|\sigma_y|\uparrow\rangle = 0$. A nonzero expectation value $\langle\sigma_y\rangle$ corresponds to a torque. Such a nonzero expectation value may arise from the perturbation by the effective vector potential:

$$\frac{\langle\uparrow|\sigma_y|\downarrow\rangle\langle\downarrow|e\boldsymbol{A}^{\mathrm{eff}}\cdot\boldsymbol{v}|\uparrow\rangle}{\mathcal{E}_\uparrow - \mathcal{E}_\downarrow} = -\frac{\sin\theta}{2}\frac{\langle\downarrow|\hbar\boldsymbol{q}\cdot\boldsymbol{v}|\uparrow\rangle}{\mathcal{E}_\uparrow - \mathcal{E}_\downarrow}. \tag{22}$$

In centrosymmetric systems response coefficients that involve one torque operator combined with an odd number of velocity operators vanish because the torque operator is parity even, while the velocity operator is parity odd. Since Eq. (22) contains only a single velocity operator, the final expression has to include one more matrix element of $e\boldsymbol{A}^{\mathrm{eff}}\cdot\boldsymbol{v}$. This matrix element is given by

$$\langle\uparrow|e\boldsymbol{A}^{\mathrm{eff}}\cdot\boldsymbol{v}|\uparrow\rangle = \hbar\frac{\cos\theta}{2}\langle\uparrow|\boldsymbol{q}\cdot\boldsymbol{v}|\uparrow\rangle. \tag{23}$$

Multiplication of Eqs. (22) and (23) shows that the dependence on q and θ is given by

$$\propto q^2\sin(\theta)\cos(\theta) \propto q^2\sin(2\theta), \tag{24}$$

in agreement with the findings in Secs. II B and II D.

F. Computational formalism

While the laser-induced adiabatic torque does not require SOI, the laser-induced nonadiabatic torque is zero in the full calculation when SOI is not included. By full calculation we mean one that considers both intrinsic and extrinsic contributions. This follows from angular momentum conservation, which is satisfied by the full calculation, provided a conserving approximation [34] is used.

In this work, we compute only the intrinsic contribution, which is nonzero even without SOI. In order to justify this approximation, we briefly recall the theory of the current-induced nonadiabatic torque, which makes use of similar approximations: The current-induced nonadiabatic torque vanishes in the absence of SOI when a conserving approximation is used. Extrinsic contributions from scattering need to be added to the intrinsic contribution in order to obtain a conserving approximation [16,17]. Therefore, the intrinsic contribution alone does not vanish in calculations without SOI. However, it has been argued that while SOI is crucial for a nonzero nonadiabatic torque, it does not strongly affect the magnitude of the nonadiabatic torque. Therefore, calculating the intrinsic nonadiabatic torque without including SOI may be useful provided there is a mechanism for angular momentum transfer to the lattice in the real system that one wishes to describe [19].

Since vertex corrections are computationally expensive and numerically tractable expressions for the vertex corrections to the laser-induced torques have not been derived yet, we consider in this work only the intrinsic laser-induced torques without SOI. Not including SOI in the calculation allows us to obtain the electronic structure of spin spirals computationally efficiently based on the generalized Bloch theorem [35]. In order to compute the laser-induced torques we employ the same equations as those used previously for collinear ferromagnets with SOI [6].

When torques are induced by femtosecond laser pulses, the torques appear retarded relative to the pulses. Retardation times between 330 fs and 3 ps have been reported [1,2]. The expressions that we derived in Ref. [6] and that we use in this work were derived under the assumption of a continuous laser beam rather than a pulse. However, a comparison between the experimental assessment of the torques induced by femtosecond laser pulses in Ref. [1] and our theory [6] showed good agreement in the magnitude of the torques. Therefore, we leave the investigation of retardation effects for future work and assess the laser-induced torques assuming a continuous laser beam in this paper.

III. RESULTS

A. Computational details

We obtain the electronic structure of bcc Fe, hcp Co, and L_10 FePt self-consistently using the density functional theory program FLEUR [36]. The lattice parameters are $a = 5.4235a_0$ (Fe); $a = 4.739a_0$, $c = 7.693a_0$ (Co); and $a = 5.1445a_0$, $c = 7.1489a_0$ (FePt), where a_0 is Bohr's radius. We apply the generalized Bloch theorem to treat the spin-spiral states [35]. In order to evaluate the laser-induced torques we take the expressions given in Ref. [6], and we make use of Wannier interpolation [37] for computational speedup. For this purpose we disentangle 18 maximally localized Wannier functions per transition metal atom, where we employ our interface [38] between FLEUR and the WANNIER90 program [39]. The Green's function formalism that we developed in Ref. [6] allows us to control disorder through a quasiparticle broadening parameter Γ, which we set to $\Gamma = 25$ meV in this paper. We set the intensity of the laser beam to $I = 10\,\mathrm{GW/cm^2}$ and the photon energy to 1.55 eV.

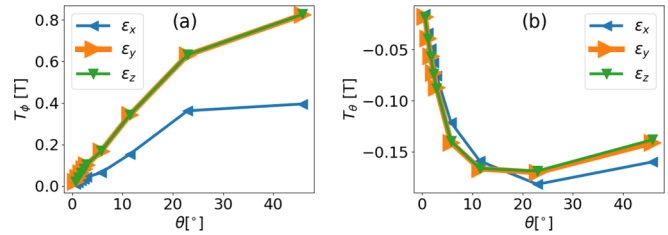

FIG. 3. Laser-induced torques in Fe vs cone angle θ when $\boldsymbol{q} = (0, -0.023, 0.023)^{\mathrm{T}}/a_0$. (a) Adiabatic torque. (b) Nonadiabatic torque.

B. bcc Fe

In Fig. 3 we show the laser-induced torques in Fe as a function of cone angle θ for q vector $\boldsymbol{q} = 0.02\boldsymbol{b}_3 = (0, -0.023, 0.023)^{\mathrm{T}}/a_0$ and the three linear polarizations $\boldsymbol{\epsilon}_x = (1, 0, 0)$, $\boldsymbol{\epsilon}_y = (0, 1, 0)$, and $\boldsymbol{\epsilon}_z = (0, 0, 1)$. Here, $\boldsymbol{b}_3$ is the reciprocal lattice vector

$$\boldsymbol{b}_3 = 2\pi \frac{\boldsymbol{a}_1 \times \boldsymbol{a}_2}{(\boldsymbol{a}_1 \times \boldsymbol{a}_2) \cdot \boldsymbol{a}_3}, \tag{25}$$

where $\boldsymbol{a}_i$ are the primitive lattice vectors. The polarizations $\boldsymbol{\epsilon}_y$ and $\boldsymbol{\epsilon}_z$ yield the same torques, while $\boldsymbol{\epsilon}_x$ yields different torques because the chosen q vector $\boldsymbol{q} = (0, -0.023, 0.023)^{\mathrm{T}}/a_0$ lies in the yz plane. For small cone angle θ both the adiabatic and nonadiabatic torques increase in magnitude with increasing θ. However, the slope decreases with increasing θ, and in the case of the nonadiabatic torque, the magnitude decreases after reaching a maximum close to 20°. This shows that the dependence on θ is not perfectly described by a simple $\sin(2\theta)$, which describes only the leading order in the expansion with respect to θ (see Sec. II B), and higher-order terms in the angular expansion are important.

In Fig. 4 we show again the laser-induced torques in Fe as a function of cone angle θ but now for a larger q vector of $\boldsymbol{q} = 0.1\boldsymbol{b}_3 = (0, -0.115, 0.115)^{\mathrm{T}}/a_0$. In this case the

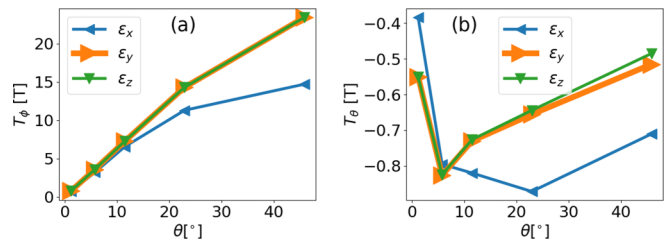

FIG. 4. Laser-induced torques in Fe vs cone angle θ when $\boldsymbol{q} = (0, -0.115, 0.115)^{\mathrm{T}}/a_0$. (a) Adiabatic torque. (b) Nonadiabatic torque.

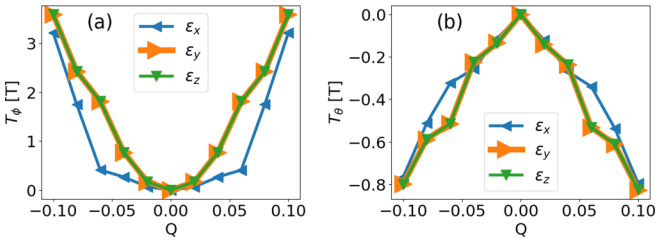

FIG. 5. Laser-induced torques in Fe vs q vector $\boldsymbol{q} = (0, -1.1585Q, 1.1585Q)^{\mathrm{T}}/a_0$ when $\theta = 5.7^\circ$. (a) Adiabatic torque. (b) Nonadiabatic torque.

nonadiabatic torque reaches a maximum already close to 5° for the polarizations $\boldsymbol{\epsilon}_y$ and $\boldsymbol{\epsilon}_z$. Compared to Fig. 3 both the adiabatic and nonadiabatic torques are larger due to the larger q. In Ref. [6] we computed the IFE and OSTT in bcc Fe and obtained 15 and 33 mT, respectively, at the same laser intensity and quasiparticle broadening as in this paper. In comparison, the adiabatic torques in Fig. 4(a) are larger by almost three orders of magnitude. We attribute these large torques to the strong SOI-like interaction from the noncollinearity discussed in Sec. II E.

In order to investigate the q dependence in more detail we show in Fig. 5 the laser-induced torques in Fe as a function of q vector $\boldsymbol{q} = Q\boldsymbol{b}_3 = (0, -1.1585Q, 1.1585Q)^{\mathrm{T}}/a_0$ when $\theta = 5.7^\circ$. The torques increase monotonously with Q, and they are even in Q. For small Q the nonadiabatic torque behaves like $\propto |Q|$, while the adiabatic torque behaves like $\propto Q^2$. This behavior is consistent with the symmetry analysis in Sec. II B predicting the torques to be even in spin-spiral wave vector q.

C. hcp Co

In Fig. 6 we show the laser-induced torques in Co as a function of cone angle θ for q vector $\boldsymbol{q} = 0.02\boldsymbol{b}_3 = (0, 0, 0.016)^{\mathrm{T}}/a_0$. The in-plane polarizations $\boldsymbol{\epsilon}_x$ and $\boldsymbol{\epsilon}_y$ yield very similar torques because the q vector points in the z direction and is therefore perpendicular to both polarizations. The slight difference between torques for $\boldsymbol{\epsilon}_x$ and $\boldsymbol{\epsilon}_y$ can be explained by considering that the x and y directions in the hexagonal unit cell are not equivalent. Similar to the case of bcc Fe shown in Fig. 3, the nonadiabatic torque attains a maximum already close to 20° and therefore requires higher-order terms in the angular expansion beyond the leading-order term $\propto \sin(2\theta)$ for its description.

In Fig. 7 we show the laser-induced torques in Co as a function of cone angle θ for the q vector $\boldsymbol{q} = 0.02\boldsymbol{b}_1 =$

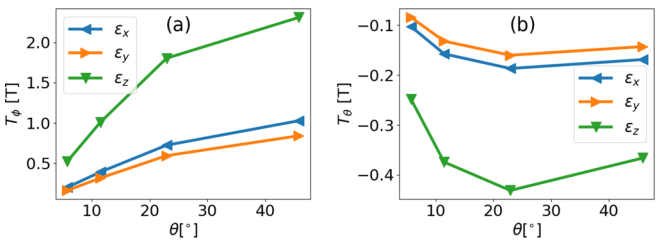

FIG. 6. Laser-induced torques in Co vs cone angle θ when $\boldsymbol{q} = (0, 0, 0.016)^{\mathrm{T}}/a_0$. (a) Adiabatic torque. (b) Nonadiabatic torque.

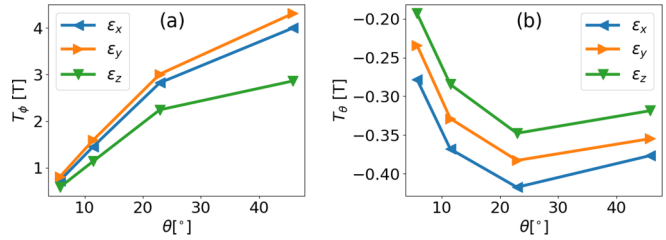

FIG. 7. Laser-induced torques in Co vs cone angle θ when $\boldsymbol{q} = (0.015, -0.0265, 0)^{\mathrm{T}}/a_0$. (a) Adiabatic torque. (b) Nonadiabatic torque.

$(0.015, -0.0265, 0)^{\mathrm{T}}/a_0$, which lies in the xy plane. The nonadiabatic torque is now different between the polarizations $\boldsymbol{\epsilon}_x$ and $\boldsymbol{\epsilon}_y$ because the q vector forms different angles with the x and y axes.

For the same laser intensity and quasiparticle broadening as used in this paper we determined the IFE and OSTT in Co in Ref. [6] and obtained 118 and 0.229 mT, respectively. In comparison, the adiabatic torques shown in Figs. 6(a) and 7(a) are orders of magnitude larger.

D. $L_1$0 FePt

In Fig. 8 we show the laser-induced torques in FePt as a function of cone angle θ for q vector $\boldsymbol{q} = 0.02\boldsymbol{b}_3 = (0, 0, 0.0176)^{\mathrm{T}}/a_0$. The torques for the polarizations $\boldsymbol{\epsilon}_x$ and $\boldsymbol{\epsilon}_y$ agree because the crystal axes a and b are equivalent and because the q vector is perpendicular to both of them. At large angles θ the adiabatic torque for polarization $\boldsymbol{\epsilon}_z$ is strongly suppressed in Fig. 8(a) due to the large anisotropy in the $L_1$0 structure. Similar to the cases of bcc Fe and hcp Co shown in Figs. 3 and 6, respectively, the nonadiabatic torque attains a maximum already close to 20° and therefore requires higher-order terms in the angular expansion beyond the leading-order term $\propto \sin(2\theta)$ for its description.

In Fig. 9 we show the laser-induced torques in FePt as a function of cone angle θ for q vector $\boldsymbol{q} = 0.02\boldsymbol{b}_1 = (0.0244, 0, 0)^{\mathrm{T}}/a_0$. In this case the torques are different for the three polarizations $\boldsymbol{\epsilon}_x$, $\boldsymbol{\epsilon}_y$, and $\boldsymbol{\epsilon}_z$: The x and y directions are inequivalent because $\boldsymbol{q}$ points in the x direction, and the z direction is inequivalent to the y direction because the c axis is longer than the b axis.

For the same laser intensity and quasiparticle broadening as used in this paper we determined the IFE and OSTT in FePt in Ref. [6] and obtained 185 and 22 mT, respectively. In

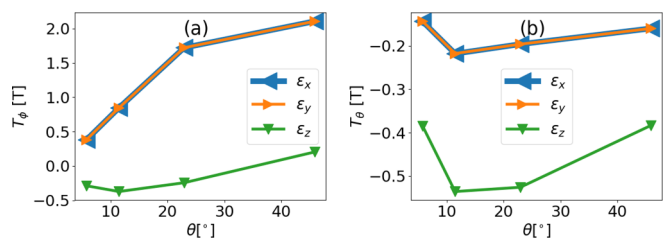

FIG. 8. Laser-induced torques in FePt vs cone angle θ when $\boldsymbol{q} = (0, 0, 0.0176)^{\mathrm{T}}/a_0$. (a) Adiabatic torque. (b) Nonadiabatic torque.

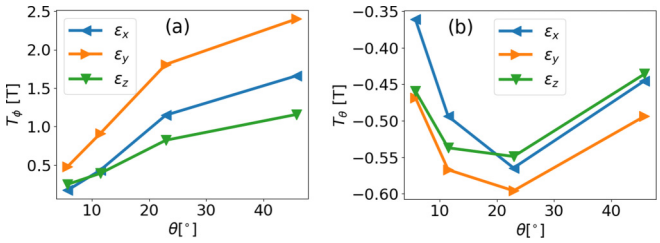

FIG. 9. Laser-induced torques in FePt vs cone angle θ when $\boldsymbol{q} = (0.0244, 0, 0.0)^{\mathrm{T}}/a_0$. (a) Adiabatic torque. (b) Nonadiabatic torque.

comparison, the adiabatic torques shown in Figs. 8(a) and 9(a) are more than one order of magnitude larger.

IV. CONCLUSION

We investigated laser-induced torques in homogeneous spin spirals without spin-orbit interaction using symmetry arguments and first-principles calculations. Symmetry analysis showed that laser-induced torques vanish for flat spirals—at the leading order of an angular expansion the dependence on spiral cone angle is $\propto \sin(2\theta)$—and that their dependence on the spin-spiral wave vector $\boldsymbol{q}$ is even in q. Additionally, it showed that laser-induced torques in homogeneous spin spirals are not associated with spin currents. Our first-principles calculations showed that the laser-induced torques in bcc Fe, hcp Co, and $L_1 0$ FePt with an imposed spin-spiral magnetic structure may be orders of magnitude larger than those in the corresponding magnetically collinear systems with SOI. This suggests that these torques may play an important role in ultrafast magnetism phenomena. Within the frozen-magnon approximation our results may also be used to estimate the laser-induced torques on magnons in these materials.

ACKNOWLEDGMENTS

We acknowledge financial support from Leibniz Collaborative Excellence project OptiSPIN–Optical Control of Nanoscale Spin Textures and funding under SPP 2137 "Skyrmionics" of the Deutsche Forschungsgemeinschaft (DFG, German Research Foundation). We gratefully acknowledge financial support from the European Research Council (ERC) under the European Union's Horizon 2020 research and innovation program (Grant No. 856538, project 3D MAGiC) and ITN Network COMRAD. The work was also supported by the DFG - TRR 173-268565370 (project A11), TRR 288-422213477 (project B06). We also gratefully acknowledge the Jülich Supercomputing Centre and RWTH Aachen University for providing computational resources under Project No. jiff40.

[1] T. J. Huisman, R. V. Mikhaylovskiy, J. D. Costa, F. Freimuth, E. Paz, J. Ventura, P. P. Freitas, S. Blügel, Y. Mokrousov, T. Rasing, and A. V. Kimel, Nat. Nanotechnol. **11**, 455 (2016).
[2] A. Capua, C. Rettner, S.-H. Yang, T. Phung, and S. S. P. Parkin, Nat. Commun. **8**, 16004 (2017).
[3] G.-M. Choi, A. Schleife, and D. G. Cahill, Nat. Commun. **8**, 15085 (2017).
[4] A. V. Kimel, A. Kirilyuk, P. A. Usachev, R. V. Pisarev, A. M. Balbashov, and T. Rasing, Nature (London) **435**, 655 (2005).
[5] P. Nemec, E. Rozkotova, N. Tesarova, F. Trojanek, E. De Ranieri, K. Olejnik, J. Zemen, V. Novak, M. Cukr, P. Maly, and T. Jungwirth, Nat. Phys. **8**, 411 (2012).
[6] F. Freimuth, S. Blügel, and Y. Mokrousov, Phys. Rev. B **94**, 144432 (2016).
[7] J. Li and P. M. Haney, Phys. Rev. B **96**, 054447 (2017).
[8] C.-H. Lambert, S. Mangin, B. S. D. C. S. Varaprasad, Y. K. Takahashi, M. Hehn, M. Cinchetti, G. Malinowski, K. Hono, Y. Fainman, M. Aeschlimann, and E. E. Fullerton, Science **345**, 1337 (2014).
[9] R. John, M. Berritta, D. Hinzke, C. Müller, T. Santos, H. Ulrichs, P. Nieves, J. Walowski, R. Mondal, O. Chubykalo-Fesenko, J. McCord, P. M. Oppeneer, U. Nowak, and M. Münzenberg, Sci. Rep. **7**, 4114 (2017).
[10] A. Manchon, J. Železný, I. M. Miron, T. Jungwirth, J. Sinova, A. Thiaville, K. Garello, and P. Gambardella, Rev. Mod. Phys. **91**, 035004 (2019).
[11] D. Ralph and M. Stiles, J. Magnet. Magn. Mater. **320**, 1190 (2008).
[12] N. Kerber, D. Ksenzov, F. Freimuth, F. Capotondi, E. Pedersoli, I. Lopez-Quintas, B. Seng, J. Cramer, K. Litzius, D. Lacour, H. Zabel, Y. Mokrousov, M. Kläui, and C. Gutt, Nat. Commun. **11**, 6304 (2020).
[13] C. Leveille *et al.*, arXiv:2007.08583.
[14] A. J. Schellekens, K. C. Kuiper, R. R. J. C. de Wit, and B. Koopmans, Nat. Commun. **5**, 4333 (2014).
[15] G.-M. Choi, C.-H. Moon, B.-C. Min, K.-J. Lee, and D. G. Cahill, Nat. Phys. **11**, 576 (2015).
[16] H. Kohno, G. Tatara, and J. Shibata, J. Phys. Soc. Jpn. **75**, 113706 (2006).
[17] R. A. Duine, A. S. Núñez, J. Sinova, and A. H. MacDonald, Phys. Rev. B **75**, 214420 (2007).
[18] I. Garate, K. Gilmore, M. D. Stiles, and A. H. MacDonald, Phys. Rev. B **79**, 104416 (2009).
[19] K.-W. Kim, K.-J. Lee, H.-W. Lee, and M. D. Stiles, Phys. Rev. B **92**, 224426 (2015).
[20] W. Töws and G. M. Pastor, Phys. Rev. Lett. **115**, 217204 (2015).
[21] E. Carpene, H. Hedayat, F. Boschini, and C. Dallera, Phys. Rev. B **91**, 174414 (2015).
[22] F. Freimuth, S. Blügel, and Y. Mokrousov, Phys. Rev. B **95**, 094434 (2017).
[23] Z. Chen and L.-W. Wang, Sci. Adv. **5**, eaau8000 (2019).
[24] S. Ghosh, F. Freimuth, O. Gomonay, S. Blügel, and Y. Mokrousov, arXiv:2011.01670.
[25] M. Finazzi, M. Savoini, A. R. Khorsand, A. Tsukamoto, A. Itoh, L. Duò, A. Kirilyuk, T. Rasing, and M. Ezawa, Phys. Rev. Lett. **110**, 177205 (2013).
[26] S.-G. Je, P. Vallobra, T. Srivastava, J.-C. Rojas-Sánchez, T. H. Pham, M. Hehn, G. Malinowski, C. Baraduc, S. Auffret, G. Gaudin, S. Mangin, H. Béa, and O. Boulle, Nano Lett. **18**, 7362 (2018).

[27] P. Olleros-Rodríguez, M. S. Strungaru, S. I. Ruta, P. I. Gavriloaea, P. Perna, R. W. Chantrell, and O. Chubykalo-Fesenko, arXiv:2011.06093.
[28] K. M. Seemann, F. Garcia-Sanchez, F. Kronast, J. Miguel, A. Kákay, C. M. Schneider, R. Hertel, F. Freimuth, Y. Mokrousov, and S. Blügel, Phys. Rev. Lett. **108**, 077201 (2012).
[29] G. Tatara, Phys. E (Amsterdam, Neth.) **106**, 208 (2019).
[30] E. Karashtin and G. Tatara, Phys. Rev. B **101**, 174439 (2020).
[31] K. Taguchi, J.-i. Ohe, and G. Tatara, Phys. Rev. Lett. **109**, 127204 (2012).
[32] F. Freimuth, S. Blügel, and Y. Mokrousov, Phys. Rev. B **96**, 104418 (2017).
[33] M. Calvo, Phys. Rev. B **18**, 5073 (1978).
[34] I. Turek, Phys. Rev. B **93**, 245114 (2016).
[35] P. Kurz, F. Förster, L. Nordström, G. Bihlmayer, and S. Blügel, Phys. Rev. B **69**, 024415 (2004).
[36] FLEUR, http://www.flapw.de.
[37] J. R. Yates, X. Wang, D. Vanderbilt, and I. Souza, Phys. Rev. B **75**, 195121 (2007).
[38] F. Freimuth, Y. Mokrousov, D. Wortmann, S. Heinze, and S. Blügel, Phys. Rev. B **78**, 035120 (2008).
[39] G. Pizzi *et al.*, J. Phys.: Condens. Matter **32**, 165902 (2020).